

Soft-Actuator-Based Robotic Joint for Safe and Forceful Interaction With Controllable Impact Response

Xiaojiao Chen , *Student Member, IEEE*, Juan Yi , *Student Member, IEEE*, Jing Li, *Student Member, IEEE*, Jianshu Zhou , *Student Member, IEEE*, and Zheng Wang , *Senior Member, IEEE*

Abstract—Impact safety and response are critical challenges for robots working under dynamic environments and with close proximity to humans. State-of-the-art rigid robots and soft robots both have limitations and tradeoffs due to their characteristics. In this letter, we introduced a hybrid-antagonistic-pneumatic joint (HAP-joint) with soft actuators and rigid structures, achieving safe and forceful interaction. Due to the hybrid approach and the wide working range of the proprietary soft actuators, the HAP-joint could achieve controllable impact responses both predetermined by control parameters and regulated online by real-time feedback. The design, modeling, control, and experimental validation of HAP-joint are presented in detail. Based on the excellent features and performances of HAP-joint, a controller framework is formulated on impact response shaping, combining passive compliance, and online regulating. The controller could achieve both excellent tracking behavior while handling accidental impacts following a desired manner, demonstrating the vast potentials of soft robots for safe and forceful interactive tasks toward various applications.

Index Terms—Human-robot interaction, pneumatic actuators, soft robotics.

I. INTRODUCTION

SERVICE robots and collaborative robots are intended to work closely with humans. From elderly-care, daily assistance, to nursing care and domestic services, the thirst for safe, efficient, and task-capable robots is tremendous and sharply increasing. With uncontrolled non-expert human users in close-proximity in potentially unstructured environments carrying out tasks with significant unmodeled portions, robots can no longer regard impacts and force exchanges with the environment and the human users as safety-concerning incidents. They must be considered as part of the normal working condition and properly handled.

Manuscript received February 24, 2018; accepted June 27, 2018. Date of publication July 9, 2018; date of current version August 2, 2018. This letter was recommended for publication by Associate Editor J. Ueda and Editor P. Rocco upon evaluation of the reviewers' comments. This work was supported in part by the Hong Kong RGC Grant 27210315 and in part by the HKU Seed Grants 201511159051, 201611159196, 201711160023, and 201711159158. (*Corresponding author: Zheng Wang.*)

The authors are with the Bionics and Control Lab, Department of Mechanical Engineering, The University of Hong Kong, Hong Kong SAR (e-mail: Chen2014@connect.hku.hk; jlicj@connect.hku.hk; yijuan@connect.hku.hk; zhoujs@connect.hku.hk; zheng.wang@ieee.org).

Digital Object Identifier 10.1109/LRA.2018.2854409

Electrical-motor based robots generally do not handle impacts very well. Intended for positioning tasks, they are often having large effective inertia, therefore hindering the passive compliance and impact safety. Recent trends enhance safety by bringing necessary active compliance control [1]–[4], or by adding passive compliant mechanism [5], [6].

Soft robotics are appealing alternatives for safe interaction [7], [8] and dexterous adaptation [9], by their ability to undergo large deformation owing to soft materials and compliant structure [10]–[12]. One of the most commonly adopted soft robotic approach utilizes pressurized expansion and selective constraining of elastomeric chambers to generate the desired deformation. Soft machines taking this approach have demonstrated excellent capability for exploring and interacting with diverse environments [13], [14]. On the other hand, soft-chamber robots are often with low-to-moderate payload, and low structural stiffness, which are important for the majority of weight-bearing tasks in daily life [15]. One promising improvement is structural enhancement to enable variable structural stiffness [16], [17]. Origami structure is also studied to get predefined shape variation [18]. However, these presents even greater challenges to modeling and control by bringing additional nonlinearity, redundancy, and structural complexity [19], [20].

Compliance and forcefulness could be obtained simultaneously, as for the linear contractile actuator Pneumatic Artificial Muscle (PAM) widely used since the 90s to achieve large payload as well as variable stiffness [21], [22]. However, the prodigious performance of PAMs is only applicable around its equilibrium point: with a maximum stroke of 35%, the peak output force occurs only at the natural resting length and decreases dramatically with the contraction [23]. These characteristics significantly restrict the usable working range and trade-offs have to be made between output torque and working range [24]. Accurate modeling of PAMs is also challenging due to nonlinearity and substantial frictions between fibers and the inflatable bladder [25].

Looking back even further, legacy pneumatic cylinders and motors provide abundant examples achieving excellent strength, linearity, compliance, and impact safety. They are widely adopted for daily tasks [26], [27]. However, their excessive size and weight, are hard to be overlooked for robotic applications today. Recent works evolved from pneumatic cylinders

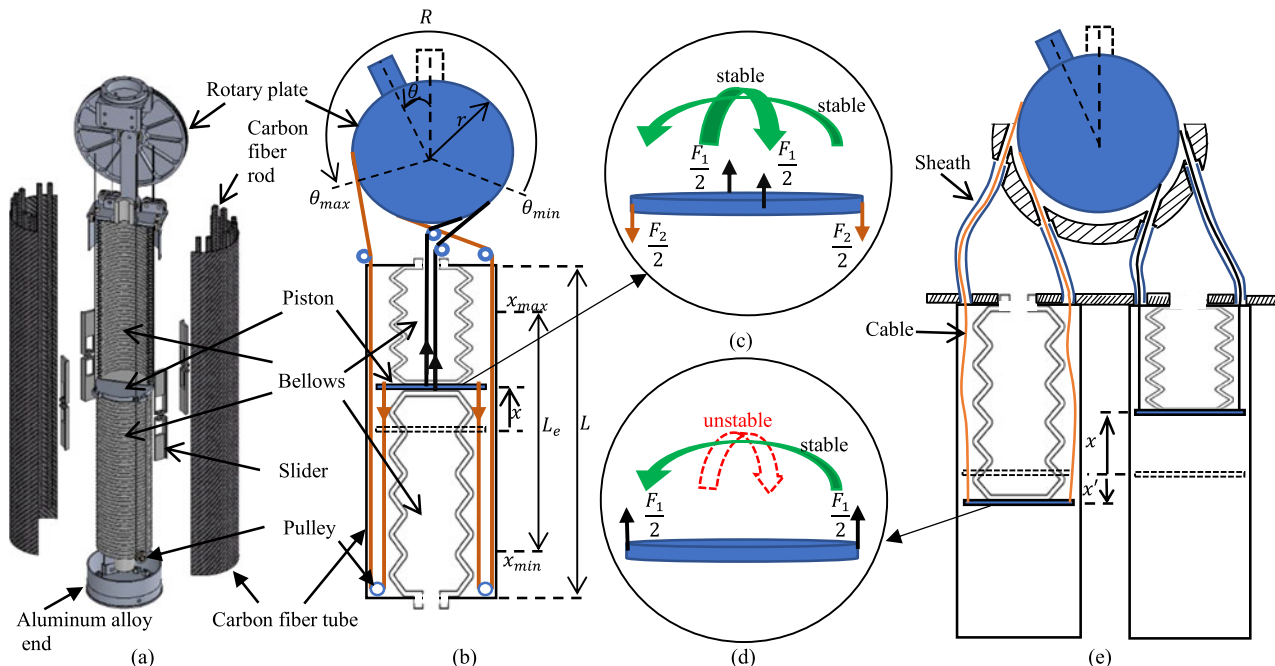


Fig. 1. (a) The mechanical design of HAP-Joint. (b) The working principle of HAP-Joint. (c) Two sets of forces with symmetric acting points make the piston of HAP-Joint stable, invulnerable to turnover. (d) Only one set of forces would cause the piston of our previous design SHELINDER vulnerable to turnover for lacking antagonistic forces in the perpendicular direction. (e) The working principle of previous design SHELINDER, using tendon-sheath mechanism. It would suffer from unequal displacement of two bellows under strong external push if inside pressure is not large.

and pneumatic motors, by using inflatable chambers to drive articulated joints antagonistically [28], [29]. For such designs with actuators integrated into the joints, payload is directly correlated to the size and weight of each joint.

Antagonistic soft robotic actuation had been explored by our previous work on a 6-DOF soft manipulator design [30]. Distinctive from state-of-the-art soft robots, we placed soft extensive actuators inside the links of the manipulator to drive articulated joints via transmission cables.

In this letter, we tackle the challenge of controllable impact behavior for strong and human-safe robots. The contribution of this letter is mainly composed of two aspects. On the hardware level, a Hybrid Antagonistic Pneumatic (HAP) robotic joint is proposed. It combines the soft chambers' low working pressure and excellent compliance, PAM's powerful and lightweight, pneumatic cylinder's large stroke and nearly linear output profile together, by using antagonistic bellows, providing a forceful output, being intrinsically safe. As a thorough redesign of our previous work in [30], HAP-Joint has improved mechanical structure and better control performance by removing tendon-sheath mechanism, halving the total volume and annealing the problem of cable relaxation subject to sudden external disturbance. On the software and control level, we proposed the idea of controllable impulse response. By combining different passive stiffness, active stiffness and integral part, different impulse behaviors were achieved, showing great potential to cope with various situations as human-being tackling with different objects. Experiments on a HAP-Joint prototype are presented, validating its characteristics, tracking performance, controllable impact response, and safety characteristics.

II. DESIGN OF THE HAP-JOINT

A. Design and Working Principle of HAP-Joint

The HAP-Joint design consists of two bellows confined collinearly in reverse direction in a carbon fiber tube with aluminum-alloy ends on both sides, as shown in Fig. 1(a). Each bellow has an air vent at one end, facing towards the outside of the tube. The closed ends face each other, between which a thin piston is stuck to both ends. Each bellow uses two cables attached at the opposing rim of the piston to transfer the force out. Two pulleys are used to redirect the cables out from the same end of the outer shell. The four cables are attached on a rotary plate to generate rotary motion, two for one direction. 16 carbon fiber rods are surrounding the bellows, forming a circular jail, making room for the passing of cables and acting as guide for piston movement.

Buckling is limited by constraining the bellows inside the carbon fiber rods jail, who confines the bellow's angular curvature within a small range. The induced friction is within acceptable range under low working pressure.

The balanced acting point of four cables in two directions gives the piston enhanced stability from turning over. As shown in Fig. 1(d), one bellow generates a force F_1 and is transmitted by two cables, represented by $\frac{F_1}{2}$ separately. These two forces make the piston stable along the line through the two acting points, but easy to turn over in the perpendicular direction. In Fig. 1(c), with the other bellow's two opposing force $\frac{F_2}{2}$ in the perpendicular direction, these four forces make the piston invulnerable to turning over in any direction.

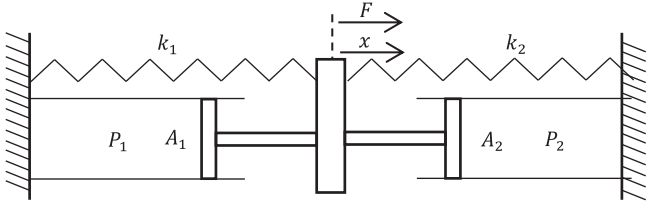


Fig. 2. The simplified force model of HAP-Joint. It would be regarded as a double-acting pneumatic cylinder with springs.

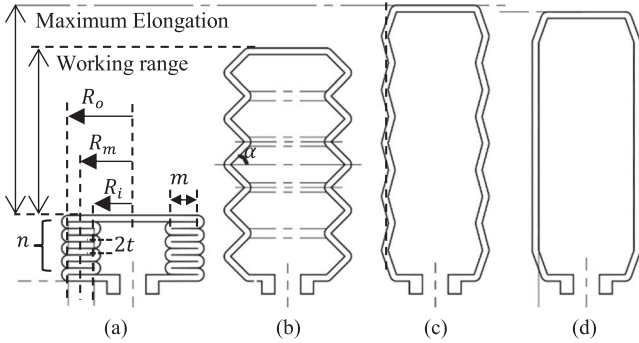


Fig. 3. V-shaped bellows used in HAP-Joint. The working range is from (a) the minimal length to its (b) free length. (c) The maximum length and (d) final length are not used.

TABLE I
PARAMETERS OF BELLOWS (LENGTH UNIT: MM)

Outer Radius (R_o)	Mean Radius (R_m)	Inner Radius (R_i)	Folding Length (m)	Segments Number (n)	Bellow Thickness (t)
≤ 33	29	≥ 25	8	41	0.7

The working principle of HAP-Joint resembles that of a pneumatic double-cylinder, as shown in Fig. 3. Opposing bellows push the inter-between piston to move, pulling the rotary joint through cables. The carefully-chosen working range inside the compression range limits the material deform within its elastic stage, avoiding plastic deformation, as shown in Fig. 2. The chosen working range of bellows in HAP-Joint is within Fig. 2(a) and (b). This helps to exhibit a linear spring force during the whole working range, except in the area near the end, where large spring rate would appear due to contacting of adjacent segments serving as a smooth hard stop. Some of the parameters of bellows used in this letter is listed in Table I, where R_o is the outer diameter, R_i is the inner diameter, R_m is the effective mean diameter, m is the length of the folding part, n is the number of total segments, t is the thickness of the bellow. The detailed parameters of the HAP-Joint in this letter are listed in Table II, and shown in Fig. 1(b).

Quite different from our previous design in [30], HAP-Joint acquires improved mechanical structure and better control performance by several significant changes. First, tendon-sheath mechanism is removed and replaced by elegantly designed pulley system. This change eliminates the problem of large friction between cable and sheath, and avoids large output force decreasing, making the position and force control realistic. Second, two

bellows of HAP-Joint are designed to be pushing a single piston opposing each other. This generates a force loop from one bellow to another bidirectionally through cables all the time, ensuring an identical displacement of two bellows. While in previous design, the cables couldn't transmit pushing force. In the case when the pressure inside the bellow is not large enough, sudden large external push may cause one bellow has smaller displacement than the other, as shown in Fig. 1(e). Another advantage is that, the piston of HAP-Joint is much more stable with four force anchoring point, compared with only two force point in previous design who is vulnerable to turn over, as shown in Fig. 1(c) and (d). HAP-Joint also becomes much more compact and lighter because the overall volume is nearly halved, as well as the corresponding supporting materials. These essential mechanical changes lay the foundation of HAP-Joint's good control performance and controllable impulse response.

B. Comparison With Other Actuators

HAP-Joint is aiming at achieving a balance between the powerful output of pneumatics and its intrinsic compliance suitable in daily task. Therefore, a low working pressure ($P = 200$ kPa) is chosen to ensure good compliance and easy daily use. Meanwhile, a large effective area ($R_m = 27$ mm) is required to provide forceful output ($F_M = 460$ N), and long stroke is needed ($L_c = 250$ mm) for adequate working range ($R = 220^\circ$).

These requirements would cause a traditional pneumatic cylinder too heavy for a light-weight human-safe robot. For example, a pneumatic cylinder from SMC lightweight MB series [31], with a bore size of 50 mm and a stroke of 250 mm, weights approximate 2 kg, while the HAP-Joint only weights less than 600 g (not including the rotary plate). This means the power-to-weight ratio of HAP-Joint is 3 times as large as that of a pneumatic cylinder. Another great advantage of HAP-Joint over pneumatic cylinder is that it has no leakage. This enables a complete shut-off of the actuator to achieve power-free blocking modes, which is impossible for a pneumatic cylinder who would continuously need high pressure source. The HAP-Joint has a fixed total length with more than 60% effective working length, while pneumatic cylinder has a changing length considering its moving rod, which is equivalent to no more than 50% contraction ratio.

The advantage of HAP-Joint over PAMs is in its more than 60% contraction ratio as well as a constantly linear output capacity, while the maximum contraction ratio of a PAM is less than 35%, and output force drops dramatically away from the equilibrium point. An industrial PAM (DMSP-40 from FESTO) [32] has only 25% contraction ratio under 200 KPa, which means trade-off must be made between output torque and enough working range. As for the weight, a pair of these PAMs is around 400 g, approximately 200 g lighter than that of HAP-Joint.

HAP-Joint is much more realistic for feedback control compared with soft-chamber robots, who suffers from lacking accurate measurements and complex continuum kinematics due to continuous deformation. The static position error of HAP-Joint could reach within 0.05° , and the tracking error is within 4° , which is hard for a soft-chamber robot to achieve. The

TABLE II
SPECIFICATIONS OF HAP-JOINT

Total Length (L)	Effective Length (L_e)	Effective Area (A_e)	Plate Radius (r)	Angle Range (R)	Working Pressure (P)	Maximum Force (F_M)	Maximum Torque (T_M)	Module Weight (w)
400mm	250mm	29mm	60mm	$(-110^\circ, 110^\circ)$	200KPa	460N	27Nm	600g

variable stiffness of soft-chamber robots is also restricted within a low range for lacking supporting structures, unable to handle disturbance-rejection situations like holding an object tight. HAP-Joint could adjust its stiffness from 6 Nm/rad with one side bellow open, to more than 40 Nm/rad, enabling very soft interaction to tight holding.

III. MODELING AND CONTROL OF HAP-JOINT

A. Modeling

1) *Modeling of HAP-Joint*: The actuation part of a HAP-Joint could be regarded as a double-acting pneumatic cylinder with a spring, as shown in Fig. 3. With a rotary plate, it generates rotational movement θ . The overall dynamics of the HAP-Joint could be written as

$$I\ddot{\theta} + G(\theta) + T_{\text{extern}} + \tau_{\text{fri}} = r(F_1 - F_2) \quad (1)$$

where I is the moment of inertia of the rotary plate, $G(\theta)$ is the gravitational term, T_{extern} is the output torque, τ_{fri} is friction, r is the radius of rotary plate, F_i is the i -th bellows output force.

Assume two bellows are identical and setup up in the same original length, then the force generated by two bellows could be written as

$$F_1 - F_2 = (P_1 - P_2) A - kx \quad (2)$$

where P_i is the internal pressure of the i -th bellow, A is the effective area, $k = 2k_0$ is the overall passive spring rate. x is related to the rotary angle θ by rotary radius r .

We use a varied friction model by introducing the effect of internal pressure accounting for the buckling effect of the bellow, represented as

$$\tau_{\text{fri}} = r \left[F_c (P_1 + P_2) \tanh\left(\frac{v}{v_1}\right) + (F_{br} - F_c (P_1 + P_2)) e^{-\alpha\left(\frac{v}{v_2}\right)^2} \right] \quad (3)$$

where, F_{br} is the breakaway friction, v_1 is the velocity threshold for coulomb friction, v_2 is the velocity threshold for striction friction, α is a tuning parameter, $F_c(P)$ is the coulomb friction related to internal pressure written as

$$F_c(P) = \beta F_{c0} \frac{P}{P_0} \quad (4)$$

where F_{c0} is the Coulomb friction in the ambient pressure P_0 , β is a coefficient experimentally determined.

The overall spring rate K and friction τ_{fri} were experimentally determined as shown in Fig. 4.

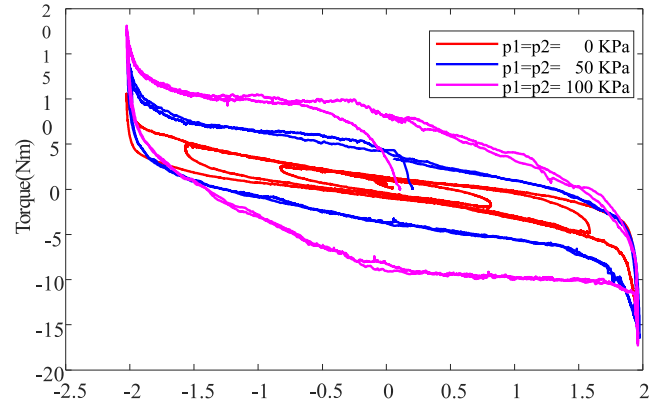


Fig. 4. Static characteristic of HAP-Joint showing a constant spring rate k and increased friction force related to internal pressure.

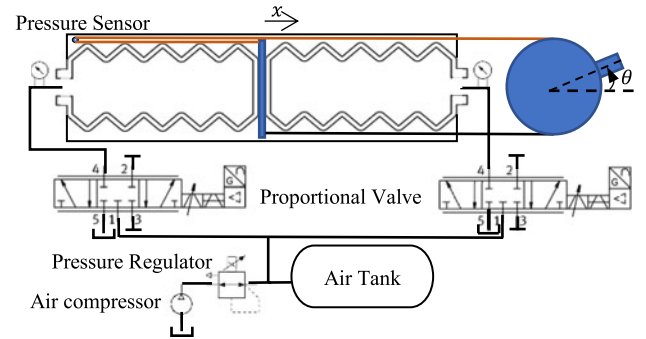


Fig. 5. Overview of the HAP-Joint pneumatic actuation system.

2) *Modeling of the Pneumatic System*: The modeling of pneumatic control system is based on the ideal gas assumption, conservation of mass and conservation of energy. In this letter, we only give a brief description of the modelling of different parts of the pneumatic system, as shown in Fig. 5.

The bellows undergoes inflating and deflating process could be regarded as adiabatic, modelled as,

$$\dot{P} = -\gamma \frac{P}{V} \dot{V} + \gamma \frac{RT}{V} \dot{m} \quad (5)$$

where P is the internal pressure, V is the below volume, γ is the heat capacity ratio for air, R is the specific gas constant for air, T is the temperature, \dot{m} is the mass flow rate.

The volume V of two bellows is given separately by

$$V_1 = rA(\theta_0 + \theta) \quad (6)$$

$$V_2 = rA(\theta_0 - \theta) \quad (7)$$

where $\theta_0 = \frac{x_0}{r}$ and x_0 is the original length of one bellow.

The proportional valve used is MPYE-5-1/8-HF-010B form FESTO, and it could be modelled as a varying area orifice whose mass flow rate is given by,

$$\dot{m} = \begin{cases} \frac{A_u C_d C_1 P_u}{\sqrt{T}} & \frac{P_d}{P_u} \leq \lambda_c \\ \frac{A_u C_d C_1 P_u}{\sqrt{T}} \sqrt{1 - \left(\frac{\frac{P_d}{P_u} - \lambda_c}{1 - \lambda_c}\right)^2} & \lambda_c < \frac{P_d}{P_u} \leq \lambda_l \\ \frac{A_u C_d C_1 P_u}{\sqrt{T}} \left(\frac{1 - \frac{P_d}{P_u}}{1 - \lambda}\right) \sqrt{1 - \left(\frac{\lambda_f - \lambda_c}{1 - \lambda_c}\right)^2} & \lambda_l < \frac{P_d}{P_u} \leq 1 \end{cases} \quad (8)$$

where \dot{m} is the mass flow rate, A_u is the opening area of the valve orifice controlled directly by voltage, C_d is the discharge coefficient, C_1 is a constant for air, λ_c is the critical pressure ratio under which the flow would be choked, typically chosen as $\lambda_f = 0.528$, $\lambda_l = 0.99$ is the pressure ratio above which the flow is assumed to be laminar.

B. Controller Design

We would like to control the position and stiffness of HAP-Joint simultaneously. Combining (1)–(5), the system dynamic equation could be rewritten as,

$$I\ddot{\theta} + k\theta + T_{ext} + G + \tau_f = RT \left(\frac{m_1}{\theta_0 + \theta} - \frac{m_2}{\theta_0 - \theta} \right) \quad (9)$$

$$\dot{m}_1 = f(u_1, P_1, P_2) \quad (10)$$

$$\dot{m}_2 = f(u_2, P_1, P_2) \quad (11)$$

where $f(u)$ is an algebraic representation of mass flow rate by input voltage with pressure feedback.

This system with relative order of 3 could be regarded as two cascaded system.

The outer position loop could be stabled by feedback linearization with PD controller, as

$$RT \left(\frac{m_1}{\theta_0 + \theta} - \frac{m_2}{\theta_0 - \theta} \right) = I\ddot{\theta}_d + k\theta_d + G(\theta_d) + \tau_f - k_p(\theta - \theta_d) - k_d(\dot{\theta} - \dot{\theta}_d). \quad (12)$$

Despite the joint angle, the HAP-Joint stiffness is given by

$$K = -\frac{\partial T_{ext}}{\partial \theta} = k + \frac{\partial G(\theta)}{\partial \theta} + \gamma RT \left(\frac{m_1}{(\theta_0 + \theta)^2} + \frac{m_2}{(\theta_0 - \theta)^2} \right). \quad (13)$$

From (12) and (13), the difference of the two pressure determines the position while the sum determines stiffness.

We could also see that the overall passive stiffness of HAP-Joint mainly composes of the original spring rate and the pneumatic spring effect. The original spring rate in HAP-Joint is about 4 Nm/rad and with pneumatic spring the stiffness could reach over 30 Nm/rad.

While many researchers treat the stiffness K as a state variable and tend to track K accurately by feedback, we regard K as an indicator or constraint, less demanding than position command.

Based on (12), (13), we obtain the desired mass command,

$$\begin{bmatrix} m_{1d} \\ m_{2d} \end{bmatrix} = \mathbf{A}^{-1} \mathbf{B}, \quad (14)$$

where

$$\mathbf{A} = \begin{bmatrix} \frac{RT}{\theta_0 + \theta} & -\frac{RT}{\theta_0 - \theta} \\ \frac{\gamma RT}{(\theta_0 + \theta)^2} & \frac{\gamma RT}{(\theta_0 - \theta)^2} \end{bmatrix}, \text{ and}$$

$$\mathbf{B} = \begin{bmatrix} I\ddot{\theta}_d + k\theta_d + G(\theta_d) + \tau_f - k_p(\theta - \theta_d) - k_d(\dot{\theta} - \dot{\theta}_d) \\ K_d - k - \frac{\partial G(\theta)}{\partial \theta} \end{bmatrix}.$$

The inner mass loop uses a P controller, and the final control law is given by

$$u_1 = f^{-1}(k_{flow}(m_1 - m_{1d})), \quad (15)$$

$$u_2 = f^{-1}(k_{flow}(m_2 - m_{2d})). \quad (16)$$

C. Controllable Impact Response

The passive stiffness K of the HAP-Joint determines the instant passive compliant behavior under expected or unexpected impact. The smaller this value, the softer the HAP-Joint would appear.

The position feedback gain term k_p could be regarded as the active stiffness. It only takes effect in the next control loop, and would only show the real effect considering the pneumatic charging process. It determines the post collision response of the joint.

The combination of the passive stiffness K and the active stiffness k_p would result in interesting impact responses, resembling that of a biology under different situations. For example, for a large passive K and a large active k_p , the joint would have little deviation and quickly settle down with little error, like a human arm holding a defending shield. In some cases, a small passive K and a large active k_p would be desired for a soft but quick recovery state, like an arm pointing at distance being disturbed by crowds. Some situation even needs both stiffness to be small, as a hand holding a full cup of water being pushed, to behave softly and submissively.

We show these controllable impact responses in the following experimental section.

IV. EXPERIMENTS VALIDATION

An embedded real-time control platform was set up for the whole experiment, as in Fig. 6. RTOS with 1ms control loop was running on an ARM Cortex M4 (STM32F429 from STMicroelectronics). The DA board (LTC2668 from Linear Technology) and AD board (ADS8588 from Texas Instruments) were both 16-bit. The pressure regulator (ITV2030L from SMC) kept the pressure in the air tank stable. The proportional valves were MPYE-5-1/8-HF-010B from FESTO. The digital pressure sensor (Honeywell HSCDANN060PGSA3) had a resolution of 60 Pa. The angle sensor (AS5048A from AMS) was 14-bit absolute magnetic encoder. The IMU (SCC2130-D08 from Murata) provided cleaner velocity than Kalman filter, and

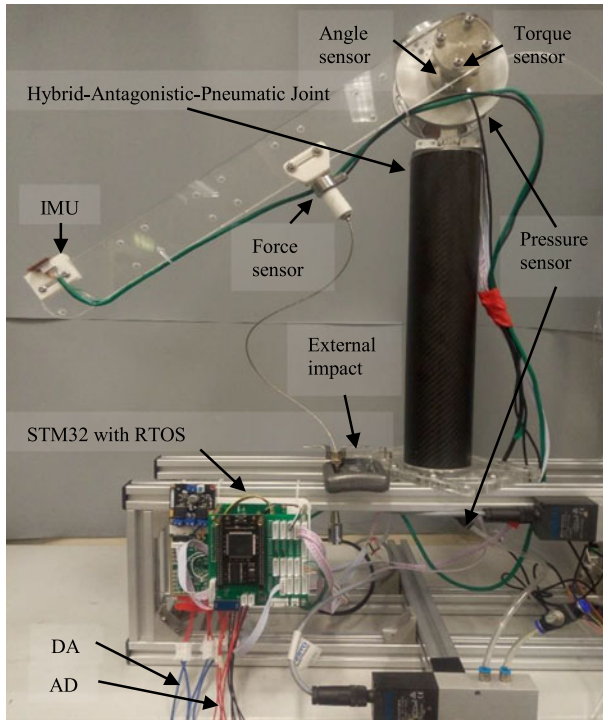


Fig. 6. Embedded real-time data acquisition and control platform.

helped determine the initial absolute angle. The torque sensor had a range of ± 30 Nm. The force sensor had a range of 0–500 N.

A. Characteristics of HAP-Joint

HAP-Joint had very good linear output profile in different positions like $\theta = -\frac{\pi}{2}$ rad, $\theta = 0$ rad and $\theta = \frac{\pi}{2}$ rad. It also had large output under low pressure. For example, a pressure of 150 kPa would generate more than 20 Nm torque, as shown in Fig. 7(b).

The variable stiffness range was large throughout the working range, as shown in Fig. 7(a). Both position $\theta = -1$ rad, $\theta = 1$ rad could have large variable stiffness from 6 Nm/rad to 30 Nm/rad with an upstream pressure of 150 kPa and output torque 1 Nm.

B. Tracking

With an upstream pressure of 200 kPa, different tracking tasks were performed.

Square wave with different amplitudes of 0.4 rad and 0.5 rad was used. The end positions were connected by S-curve for smooth transitions. The outcome showed excellent tracking performance of the HAP-Joint as shown in Fig. 8(a).

Sinusoidal references with different frequencies of 0.5 Hz and 1 Hz were also tested, shown in Fig. 8(b). The results showed good tracking ability.

C. Controllable Impact Response

Four combinations of passive stiffness K and active stiffness k_p were compared in a falling impact test. The falling mass was

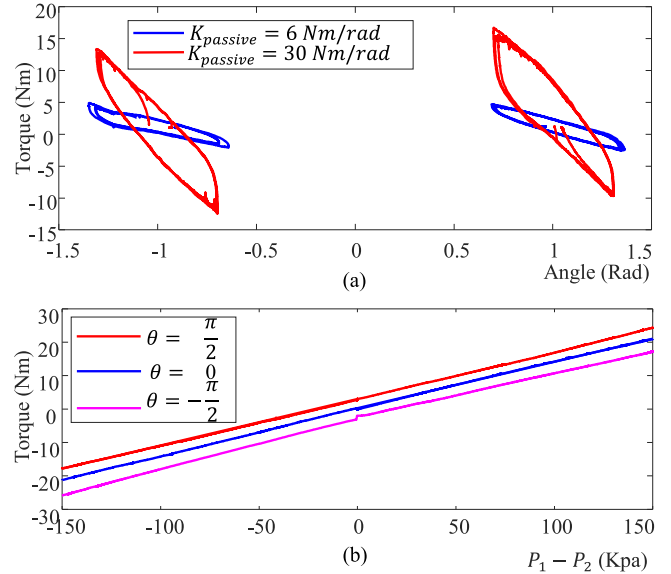


Fig. 7. (a) Variable stiffness throughout the working range. (b) Linear output profile with large output and large working range.

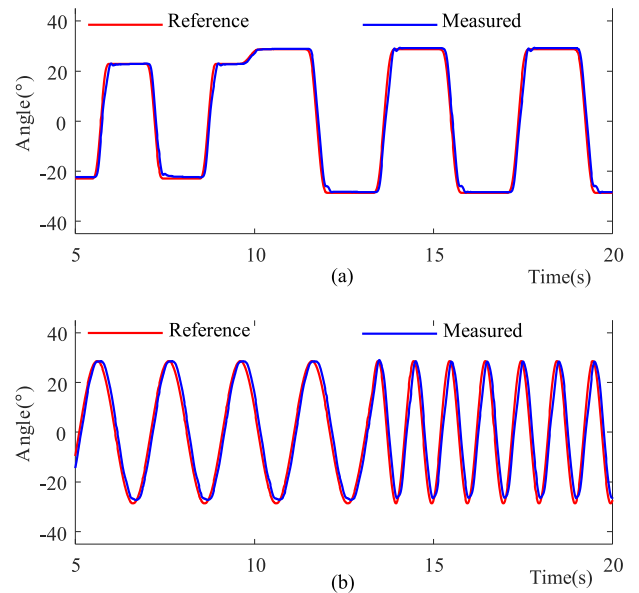


Fig. 8. (a) Square wave tracking with different amplitudes. (b) Sinusoidal wave with different frequencies tracking.

1.5 kg and the height was 0.1 m, the contacting arm was 0.2 m. Recorded angle and torque were shown in Fig. 9.

In Fig. 9(a) and (b), with small passive stiffness $K = 16$ Nm/rad, the instantaneous angle achieved more than 0.2 rad, and the maximum torque was 5 Nm. In Fig. 9(c) and (d), the passive stiffness $K = 30$ Nm/rad, the angle deviation was only 0.02 rad, and the resulting impact torque doubled to 10 Nm.

In Fig. 9(a), a small active stiffness $k_p = 1$ left a large steady-state deviation, while in Fig. 9(b), the steady-state deviation was much smaller when $k_p = 150$.

With the adding of integral part in the active control, more bio-resembling behavior could be achieved, as shown in Fig. 10. The joint would return to original by integral while maintaining

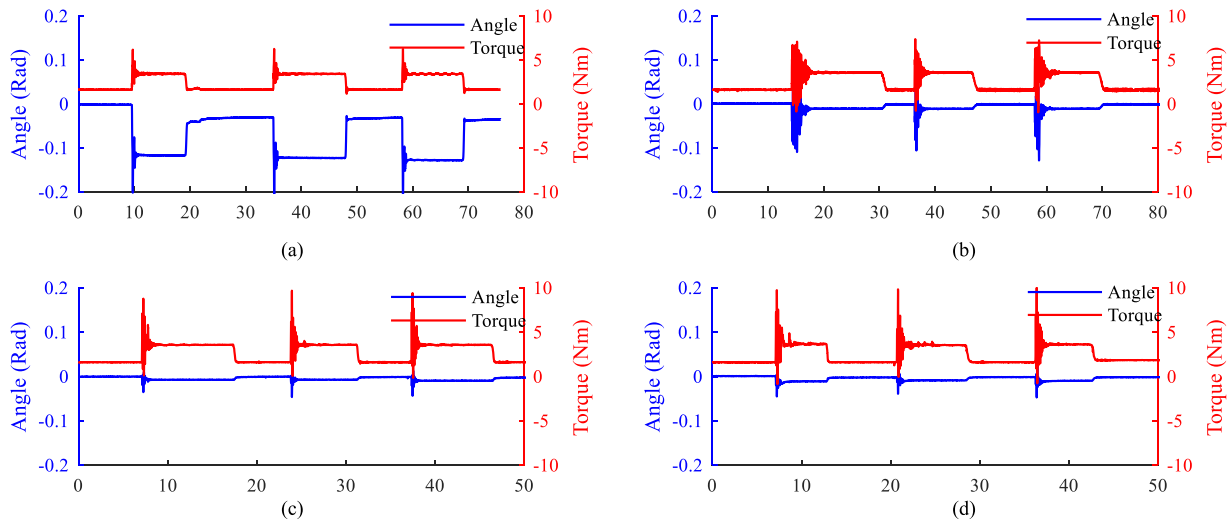


Fig. 9. Controllable impact response with different passive K and active k_p . (a) Small passive K , small active k_p . (b) Small passive K , large active k_p . (c) Large passive K , small active k_p . (d) Large passive K , large active k_p .

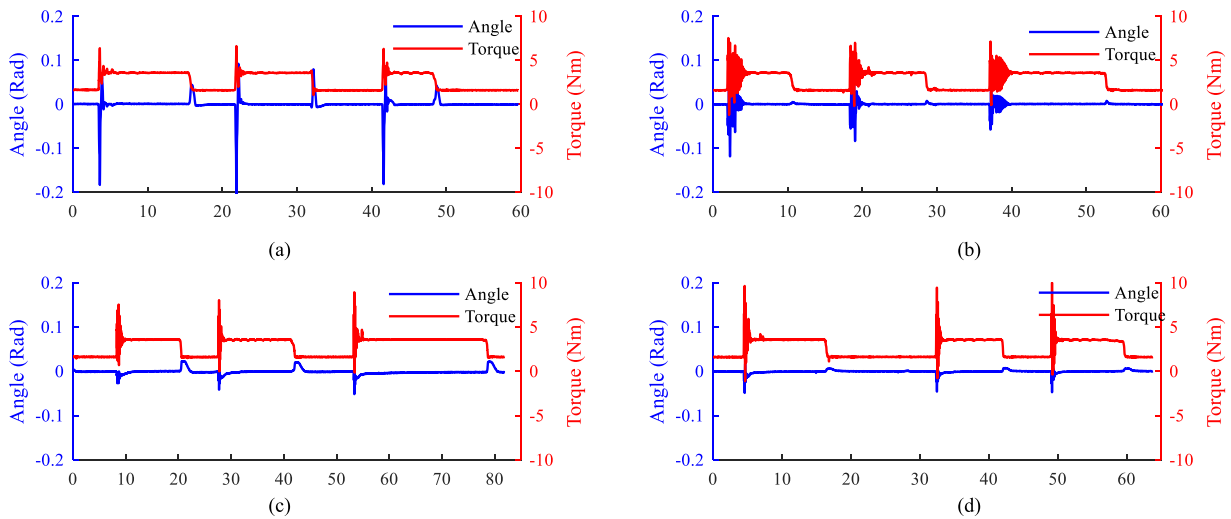


Fig. 10. Controllable impact response with different passive K and active k_p and integral part. (a) Small passive K , small active k_p , with integral part. (b) Small passive K , large active k_p , with integral part. (c) Large passive K , small active k_p , with integral part. (d) Large passive K , large active k_p , with integral part.

the passive and active capability determined by passive K and active k_p .

These experiments showed HAP-Joint's controllable impact response by adjusting passive stiffness and active stiffness, displaying great potential for a safe bio-mimic robotic arm.

D. Safety Characteristic

Safety is a paramount concern in human-robot interaction. HAP-Joint is totally safe to humans by its low working pressure.

Several safety indices exist concerning human-robot interaction, including the Gadd Severity Index (GSI) and the head Injury Criterion (HIC). Both GSI and HIC is based on a measurement of impact pulse using head acceleration, which is hard to acquire. Another simple approach is to measure the impulse force from the manipulator's side. A smaller impulse

peak force would always mean a safer manipulator. We took this approach in this experiment.

The influence of passive stiffness K and active k_p on the safety characteristic of HAP-Joint was investigated by first recording the reference peak torque with the HAP-Joint fixed and then measuring the peak torques under different sets of passive stiffness K and active k_p , 10 times for each set. The result is shown in Fig. 11. The passive stiffness K has a strong influence on the peak torque while the active k_p doesn't contribute much to the lessening of peak torque. This result indicates that the pressures inside bellows are important for passive interaction, while active control would fail to timely soften the impulse interaction due to inflating or deflating delay. This experiment demonstrates the intrinsic safety characteristic of HAP-Joints, and validates our choice of adopting low working pressure for safer interaction.

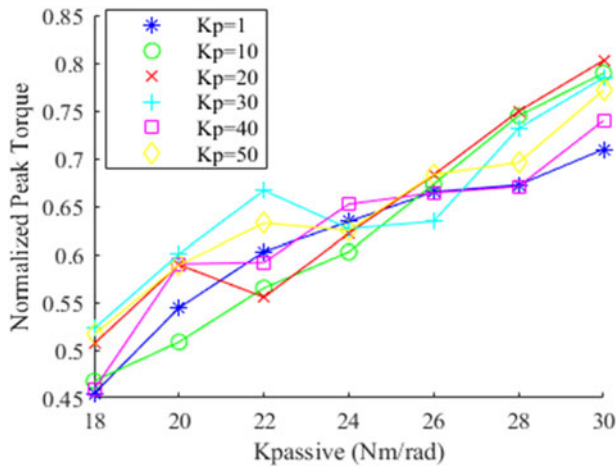


Fig. 11. The influence of passive stiffness K and active k_p on the peak torque.

V. CONCLUSION

In this letter, a Hybrid Antagonistic Pneumatic (HAP) robotic joint was proposed, with low working pressure, excellent compliance, linear output characteristics, high payload, and lightweight. The HAP-Joint is intrinsically safe for both expected and unexpected interactions. Modeling and control on variable stiffness and impact behavior shaping were investigated and discussed. Experiments on a fabricated HAP-Joint prototype were presented, validating its characteristics, safety, tracking performance and demonstrating the controllable impact responses following different strategies.

This work provides insights on a preemptive approach to impact behavior shaping: by strategically setting the air pressures in the joint chambers, the robot could have pre-defined impact response behavior without immediate controller intervention. Moreover, we have demonstrated that this could be very-well integrated with the conventional control laws such as PID widely used in today's robotic control practices.

REFERENCES

- [1] N. Hogan, "Impedance control: An approach to manipulation: Part I—Theory," *J. Dyn. Syst. Meas. Control*, vol. 107, no. 1, pp. 1–7, 1985.
- [2] H. Sadeghian, L. Villani, M. Keshmiri, and B. Siciliano, "Task-space control of robot manipulators with null-space compliance," *IEEE Trans. Robot.*, vol. 30, no. 2, pp. 493–506, Apr. 2014.
- [3] A. Albu-Schäffer and G. Hirzinger, "Cartesian impedance control techniques for torque controlled light-weight robots," in *Proc. IEEE Int. Conf. Robot. Automat.*, May 2002, pp. 657–663.
- [4] Z. Wang, A. Peer, and M. Buss, "Fast online impedance estimation for robot control," in *Proc. IEEE Int. Conf. Mechatronics*, Apr. 2009, pp. 1–6.
- [5] B. Vanderborght *et al.*, "Variable impedance actuators: A review," *Robot. Auton. Syst.*, vol. 61, no. 12, pp. 1601–1614, 2013.
- [6] N. Paine, S. Oh, and L. Sentis, "Design and control considerations for high-performance series elastic actuators," *IEEE/ASME Trans. Mechatronics*, vol. 19, no. 3, pp. 1080–1091, Jun. 2014.
- [7] J. Zhou, J. Yi, X. Chen, Z. Liu, and Z. Wang, "BCL-13: A 13-DOF Soft robotic hand for dexterous grasping and in-hand manipulation," *IEEE Robot. Automat. Lett.*, vol. PP, no. c, pp. 1–1, 2018.
- [8] J. Yi, X. Chen, and Z. Wang, "A three-dimensional-printed soft robotic glove with enhanced ergonomics and force capability," *IEEE Robot. Autom. Lett.*, vol. 3, no. 1, pp. 242–248, Jan. 2018.
- [9] J. Zhou, S. Chen, and Z. Wang, "A soft-robotic gripper with enhanced object adaptation and grasping reliability," *IEEE Robot. Autom. Lett.*, vol. 2, no. 4, pp. 2287–2293, Oct. 2017.
- [10] J. Zhou, X. Chen, J. Li, Y. Tian, and Z. Wang, "A soft robotic approach to robust and dexterous grasping," *IEEE Int. Conf. Soft Robot.*, vol. 5, no. 200, pp. 412–417, 2018.
- [11] S. Kim, C. Laschi, and B. Trimmer, "Soft robotics: A bioinspired evolution in robotics," *Trends Biotechnol.*, vol. 31, no. 5, pp. 287–294, 2013.
- [12] C. Majidi, "Soft robotics: A perspective—Current trends and prospects for the future," *Soft Robot.*, vol. 1, no. 1, pp. 5–11, 2014.
- [13] B. Mosadegh *et al.*, "Pneumatic networks for soft robotics that actuate rapidly," *Adv. Functional Mater.*, vol. 24, no. 15, pp. 2163–2170, 2014.
- [14] Z. Shen, J. Na, and Z. Wang, "A biomimetic underwater soft robot inspired by cephalopod mollusc," *IEEE Robot. Autom. Lett.*, vol. 2, no. 4, pp. 2217–2223, Oct. 2017.
- [15] M. Manti, V. Cacucciolo, and M. Cianchetti, "Stiffening in soft robotics: A review of the state of the art," *IEEE Robot. Autom. Mag.*, vol. 23, no. 3, pp. 93–106, Sep. 2016.
- [16] Y. Li, Y. Chen, Y. Yang, and Y. Wei, "Passive particle jamming and its stiffening of soft robotic grippers," *IEEE Trans. Robot.*, vol. 33, no. 2, pp. 446–455, Apr. 2017.
- [17] Y. Wei, Y. Chen, Y. Yang, and Y. Li, "A soft robotic spine with tunable stiffness based on integrated ball joint and particle jamming," *Mechatronics*, vol. 33, pp. 84–92, 2016.
- [18] J. Yi, X. Chen, C. Song, and Z. Wang, "Fiber-reinforced origami robotic actuator," *Soft Robot.*, vol. 5, no. 1, pp. 81–92, 2017.
- [19] Z. Wang, P. Polygerinos, J. T. B. Overvelde, K. C. Galloway, K. Bertoldi, and C. J. Walsh, "Interaction forces of soft fiber reinforced bending actuators," *IEEE/ASME Trans. Mechatronics*, vol. 22, no. 2, pp. 717–727, Apr. 2017.
- [20] Z. Wang, Z. Sun, and S. J. Phee, "Haptic feedback and control of a flexible surgical endoscopic robot," *Comput. Methods Programs Biomed.*, vol. 112, no. 2, pp. 260–271, 2013.
- [21] B. Tondu, "A seven-degrees-of-freedom robot-arm driven by pneumatic artificial muscles for humanoid robots," *Int. J. Robot. Res.*, vol. 24, no. 4, pp. 257–274, 2005.
- [22] B. Vanderborght, R. Van Ham, B. Verrelst, M. Van Damme, and D. Lefeber, "Overview of the Lucy project: Dynamic stabilization of a biped powered by pneumatic artificial muscles," *Adv. Robot.*, vol. 22, no. 10, pp. 1027–1051, 2008.
- [23] B. Tondu and P. Lopez, "Modeling and control of McKibben artificial muscle robot actuators," *IEEE Control Syst. Mag.*, vol. 20, no. 2, pp. 15–38, Apr. 2000.
- [24] D. Shin, X. Yeh, and O. Khatib, "Circular pulley versus variable radius pulley: Optimal design methodologies and dynamic characteristics analysis," *IEEE Trans. Robot.*, vol. 29, no. 3, pp. 766–774, Jun. 2013.
- [25] B. Tondu, "Modelling of the McKibben artificial muscle: A review," *J. Intell. Mater. Syst. Struct.*, vol. 23, no. 3, pp. 225–253, 2012.
- [26] J. Wang, J. Pu, and P. Moore, "Accurate position control of servo pneumatic actuator systems: an application to food packaging," *Control Eng. Pract.*, vol. 7, no. 6, pp. 699–706, Jun. 1999.
- [27] FESTO, "BionicCobot—Sensitive helper for human-robot collaboration," FESTO AG & Co. KG, Esslingen, Germany, 2017.
- [28] J. Fras, Y. Noh, H. Wurdemann, and K. Althoefer, "Soft fluidic rotary actuator with improved actuation properties," in *Proc. IEEE/RSJ Int. Conf. Intell. Robot. Syst.*, Sep. 2017, pp. 5610–5615.
- [29] A. Dameitry and H. Tsukagoshi, "Lightweight underactuated pneumatic fingers capable of grasping various objects," in *Proc. IEEE Int. Conf. Robot. Automat.*, Jun. 2016, pp. 2009–2014.
- [30] X. Chen, J. Peng, J. Zhou, Y. Chen, M. Y. Wang, and Z. Wang, "A robotic manipulator design with novel soft actuators," in *Proc. IEEE Int. Conf. Robot. Automat.*, 2017, pp. 1878–1884.
- [31] SMC, "Air cylinder MB series," 2018. [Online]. Available: http://ca01.smcworld.com/catalog/en/actuator/MB-MDB-Z-E/6-2-1-p0387-0434-mb_en/data/6-2-1-p0387-0434-mb_en.pdf, Accessed on: May 30, 2018.
- [32] Festo AG, "Datasheet—DMSP fluidic muscle DMSP/MAS," 2016. [Online]. Available: https://www.festo.com/rep/en_corp/assets/pdf/info_501_en.pdf, Accessed on: May 30, 2018.